frontiers | Frontiers in Earth Science

TYPE Original Research
PUBLISHED 20 November 2024
DOI 10.3389/feart.2024.1503158

OPEN ACCESS

EDITED BY
Jihoon Kim,
Texas A and M University, United States

REVIEWED BY
Huajin Li,
Chengdu University, China
Zhengzheng Cao,
Henan Polytechnic University, China

*CORRESPONDENCE
Xilin Shi,
xlshi@whrsm.ac.cn

RECEIVED 28 September 2024
ACCEPTED 05 November 2024
PUBLISHED 20 November 2024

CITATION
Huang S, Lu J, Wang J, Fu X, Fu Y, Li Y, Shi X, Dong Z, Zhao K, Li P, Xu M and Chen X (2024) Experimental study on creep characteristics of electrolyte-bearing salt rock under long-term triaxial cyclic loading.
Front. Earth Sci. 12:1503158.
doi: 10.3389/feart.2024.1503158

Experimental study on creep characteristics of electrolyte-bearing salt rock under long-term triaxial cyclic loading

Si Huang[1,2], Jun Lu[3], Jian Wang[3], Xinghui Fu[4], Yaping Fu[3], Yinping Li[1,2,5], Xilin Shi[1,2]*, Zhikai Dong[6], Kai Zhao[1,2], Peng Li[1,2], Mingnan Xu[1,2] and Xiangsheng Chen[7]

[1]State Key Laboratory of Geomechanics and Geotechnical Engineering, Institute of Rock and Soil Mechanics, Chinese Academy of Sciences, Wuhan, China, [2]University of Chinese Academy of Sciences, Beijing, China, [3]PipeChina Energy Storage Technology Co., Ltd., Shanghai, China, [4]Jiangsu Suyan Jingshen Co., Ltd., Huai'an, China, [5]Hubei Key Laboratory of Geo-Environmental Engineering, Institute of Rock and Soil Mechanics, Chinese Academy of Sciences, Wuhan, China, [6]School of Safety Engineering and Emergency Management, Shijiazhuang Tiedao University, Shijiazhuang, China, [7]School of Civil Engineering and Architecture, East China Jiaotong University, Nanchang, China

During the operation of the Salt Cavern Flow Battery (SCFB) system, the rock surrounding a salt cavern is subjected to erosion by the electrolyte. To study the creep characteristics of electrolyte-bearing salt rock under long-term triaxial cyclic loading in SCFB, a triaxial creep experiment with a cycle period of 1 day was conducted. The results indicated that, when not subjected to failure, the axial stress-strain curve of electrolyte-bearing sample undergoes only two phases of "sparse-dense", entering dense phase approximately 4 cycles earlier than that of sample without electrolyte. Under the same stress conditions, the strain generated in electrolyte-bearing salt rock surpasses that of sample without electrolyte, demonstrating an initial rapid increase followed by a gradual stabilization trend. The stress-strain curve of electrolyte-bearing sample in a single cycle can be divided into six stages. The number of cycles has almost no effect on the axial strain in stages I, IV, V and VI, and the axial strain in stages IV and VI is basically 0. Additionally, the elastic deformation generated in stage I is basically recovered in stage V. The strain in stage II gradually decreases and disappears in the 4th cycle, which is 13 cycles earlier than that of the sample without electrolyte. The creep rate of electrolyte-bearing sample shows a trend of "gradual decrease—basically stabilization" as the number of cycles increases, and the creep experiment contains only the decay creep stage and steady creep stage. Irreversible deformation of electrolyte-bearing sample exhibits a gradual decrease followed by stabilization with increasing number of cycles. The research findings hold significant implications for the stability analysis of SCFB systems.

KEYWORDS

salt rock, creep characteristics, triaxial cyclic loading, elastic modulus, stress-strain curve

1 Introduction

Against the backdrop of environmental pollution caused by traditional fossil fuels and the growing global energy demand, renewable energy has garnered significant attention in recent years (Beh et al., 2017; Cao et al., 2024e; Li H. et al., 2019; McGlade and Ekins, 2015), such as wind and solar power. However, the intermittency and variability of renewable energy pose significant security risks to large-scale integrated power grids (Cao et al., 2024d; Chen et al., 2021; Dunn et al., 2011; Li et al., 2022b; Wang et al., 2024). Energy storage technologies have emerged as one effective solution to address this issue (Ambrose et al., 2023; Cao et al., 2024c; Zhang et al., 2016). Among these, flow battery energy storage technology has emerged as a prominent contender due to its notable advantages including high safety, long cycle life, and flexible design (Cao et al., 2020; Gentil et al., 2020; Montero et al., 2022). Consequently, it has distinguished itself among numerous energy storage technologies as one of the more mature options currently available (Cao et al., 2024b; DeBruler et al., 2017; Kwabi et al., 2020; Li et al., 2022a). However, flow battery energy storage currently faces three main shortcomings: electrolyte storage tanks are arranged on the ground, covering a large area; the electrolyte working environment needs constant temperature, and the cost of heat preservation is significant; and it is easy to become a target of attack in wartime (Cao et al., 2024a; Li et al., 2018; Wang H. et al., 2021; Wei et al., 2024; Zhang et al., 2020). Underground salt cavern reservoirs are dissolved cavities formed in deep-seated salt mines through solution mining (Hongwei et al., 2018; Huang et al., 2023; Li et al., 2020; Shi et al., 2018; Yang H. et al., 2023). The properties of salt rock itself, such as low permeability, high plastic deformation capacity, excellent creep behavior, and self-healing damage (Kolano et al., 2024; Li H. et al., 2023; Liu et al., 2022; Mishra and Makov, 2022; Peng et al., 2020; Wang et al., 2023; Wang et al., 2022; Yang Y. et al., 2023), provide underground salt cavern reservoirs with relatively stable environmental temperatures, excellent sealing characteristics, and resistance to damage, making them one of the internationally recognized methods for hydrocarbon storage (Chen et al., 2013; Fan et al., 2017; Ma et al., 2022; Vandeginste et al., 2023; Wei et al., 2016; Wei et al., 2023). Therefore Shi et al. (2023), proposed a novel salt cavern flow battery (SCFB) system (Figure 1) that can address the three shortcomings mentioned above. The SCFB system utilizes a saturated NaCl solution as supporting electrolyte, with salt cavern serving as storage location for electrolyte. In a system where electrolyte of different valence states are stored at the same electrode within a single salt cavern, the concentration of a single valence state electrolyte tends to become excessively low and unevenly distributed. Therefore, this system deploys two or more salt caverns separately at the positive or negative electrodes, with each cavern dedicated to storing a single valence state electrolyte as much as possible. This approach enhances the concentration of the same valence state electrolyte within the salt caverns, thereby improving the energy density and efficiency of SCFB during discharge.

There are various types of flow batteries, but not all are suitable for storage in salt caverns. For instance, the all-vanadium flow battery with a strong acid-based supporting electrolyte is not suitable for storage in salt caverns due to the potential for serious underground contamination caused by the robust acid solution

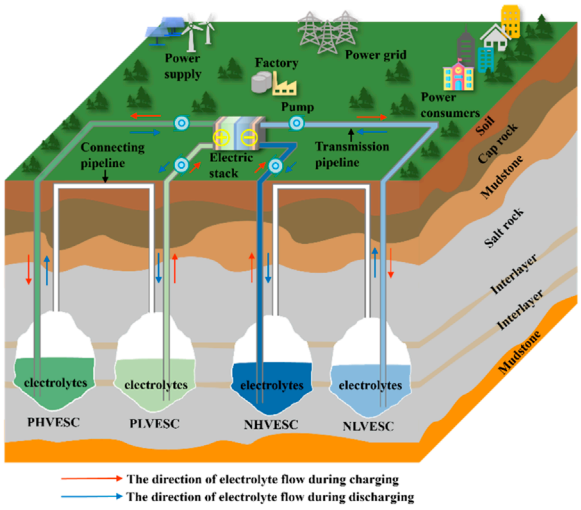

FIGURE 1
Schematic diagram of a new salt cavern liquid flow battery system.

(Zhou et al., 2024). Similarly, strong alkaline electrolyte are also unsuitable for storage in salt caverns (Bao et al., 2024). Wang H. et al. (2021) proposed that a neutral aqueous flow battery composed of a saturated NaCl solution as the supporting electrolyte, N,N,N, 2,2,6,6-heptamethylpiperidinyloxy (TEMPO) as the catholyte, and 1,1-di-methyl-4,4-bipyridilium (MV) as the anolyte is suitable for storage in salt caverns. While this patent (Shi et al., 2023) addresses some issues related to the SCFB system, the creep characteristics of electrolyte-bearing salt rock have a strong connection to the long-term stability of SCFB operation. During the operation of SCFB systems, the surrounding rock around the salt cavern is in direct contact with the electrolyte. Whereas salt caverns currently store mainly oil, gas and air, the working conditions faced by SCFB are different from those of them (Voznesenskii et al., 2017). Additionally, as the electrolyte in the SCFB system is cyclically injected or withdrawn, the surrounding rock in the salt cavern is equivalent to undergoing cyclic loading and unloading, this process may persist for an extended period (Li T. et al., 2019). Therefore, elucidating the creep characteristics of electrolyte-bearing sample under long-term triaxial cyclic loading is crucial. This helps to analyze the long-term stability of SCFB systems.

Numerous scholars have studied the creep characteristics of salt rock under certain conditions. Fuenkajorn and Phueakphum (Fuenkajorn et al., 2009) investigated the creep characteristics of salt rock taken on site under cyclic loading, and the results showed that compressive strength of the salt rock shows a gradual decreasing trend as the cycle period increases. The elastic modulus of salt rock decreases insignificantly at the beginning of cycles, then slowly tends to a stabilization phase, and finally continues until failure Ma et al. (2013) studied the evolution law of mechanical characteristics of salt rock subjected to triaxial cyclic loading. The research results indicated that the elastic modulus of samples shows a gradual decreasing trend as the loading period increases, and the decreasing trend is exponential. Under cyclic loading in the presence of confining stress, both axial and lateral deformations of salt rock exhibit transient and steady-state evolutionary patterns.

This behavior is analogous to that observed in conventional static creep experiments. As the stress level applied to the sample increases, the strain generated during transient creep phase gradually increase, which increase the proportion of the total accumulated strain. Wang J. et al. (2021) studied that the creep characteristics of salt rock subjected to cyclic loading with single cycles ranging from 1 to 8 h. The results showed that maximum creep rate of samples first gradually decreases, then tends to stabilize, and finally gradually increases the trend with loading cycles. Similarly, the creep process of samples shows a similar three-stage characteristic. During the experimentation, it was observed that in the maximum cyclic stress condition, a critical threshold is present for cycles. If this critical threshold is not exceeded, the cyclic life of the salt rock will be prolonged, resulting in a more significant amount of creep deformation Liu et al. (2013). investigated the damage development law of salt rock under cyclic loading. It was also pointed out that a critical value for the maximum stress level applied to the sample is observed to be 40% of the uniaxial compressive strength of the sample. When the maximum stress level exceeds this critical value, there is a significant tendency for the damage obtained from the sample to increase. Zhao et al. (2022) studied the damage development laws of salt rock under stepwise increasing stress levels. The results showed that the shape of the hysteresis loops of the single-cycle creep curves of the samples is strongly correlated with the applied stress level Fan et al. (2016). comparatively studied the difference between the effects of conventional and interval fatigue tests on fatigue activity in samples. The results indicated that in these two types of fatigue experiments, it was observed that the residual strain of the sample in conventional fatigue experiments is significantly smaller than that in interval fatigue experiments. The single-cycle interval time has a strong effect on the irreversible deformation of the samples. Dong et al. (2023) studied the impact of different temperatures on the creep characteristics of salt rock samples taken from depths below 2,000 m. The results indicated that as the temperature level increases, the transient creep duration of sample gradually decreases, but the steady-state creep rate of sample gradually increases. The time required for the sample to creep into the volume dilatation stage is also less when the temperature level increases.

Furthermore, to better simulate the working situations of salt caverns in the field, The creep behavior of salt rock during cyclic loading and unloading tests with single cycle periods of 1 day and 7 days was investigated in this doctoral thesis (Dong, 2023). The doctoral thesis revealed that during the initial stage of axial deviatoric stress rise in the first cycle, the creep deformation of salt rock samples with a single cycle period of 7 days is greater than that of sample with a single cycle period of 1 day. This is different from the findings of Wang J. et al. (2021). Discrepancy may be attributed to the excessively short single cycle period in the experiments of Wang J. et al. (2021), where creep deformation of salt rock is relatively small compared to elastic deformation induced by compression, thus not significantly influencing the total deformation at this stage Lyu et al. (2021). investigated the creep characteristics of salt rock during ultra-long period through creep experiments lasting 2,100 h (875 days). The results showed that compared with conventional high stress creep experiments, the first stage of creep of the sample will be longer, about 4.3–8.3 months. Bérest et al. (2019). used a gallery in the Altaussee salt mine in Austria to study the creep characteristics of on-site salt rocks within a small deviatoric stress range (0.2–0.6 MPa) for a period of 2 years. The results indicated that the transient creep stage of salt rock within the small deviatoric stress range lasts longer than that within the high stress range, about 6–10 months. The steady state strain rates observed in real time are 7–8 orders of magnitude higher than those in the high stress range Guessous et al. (1987) studied the effect of on-site disturbances on salt rock creep by radially compressing salt rock samples before conducting creep experiments. The experimental results indicated that in the early stage of the experiment, it was observed that the preloading history had a significant impact on the creep behavior of salt rock. The degree of this influence depends on the radial compression strength before the experiment.

However, there have been no reports on the study of creep characteristics of electrolyte-bearing salt rock under long-term triaxial cyclic creep experiments. Therefore, this study employed a TEMPO with a saturated NaCl solution as the supporting electrolyte, utilizing a self-developed device for soaking salt rock samples in electrolyte through the test equipment for high-temperature and high-pressure medium soaking of surrounding rock in salt cavern storage. Subsequently, single-cycle creep tests with a duration of 1 day were conducted using a deep salt rock ultra-low frequency cyclic loading creep test system. The experimental results of single-cycle creep tests on salt rock without electrolyte serve as a reference, taken from data in the doctoral thesis of our research group (Dong, 2023). The effect of the electrolyte-bearing state on the long-term creep behavior of salt rock was analyzed. These findings contributed to a better understanding of the creep properties of electrolyte-bearing salt rock in SCFB, holding significant implications for stability analysis of SCFB reservoir.

2 Experimental materials and methods

2.1 Sample preparation

The salt rock sample used in this experiment was obtained from the same core as the sample used in this doctoral thesis (Dong, 2023), extracted at a depth of 1,459 m. The reason why both samples were taken from the same core is that this minimizes the impact on the experimental results due to the inhomogeneity between the samples. Therefore, it is assumed here that the properties of these two samples are the same. Prior to any processing, the samples did not undergo any loading. Since the salt rock samples in this paper are taken from the salt mines in the field, it is inevitable that some impurities exist in the samples. This sampling method is more meaningful for guiding the engineering site. X-ray diffraction (XRD) was used to analyze the composition of the samples in more detail. The results showed that the key contributors of the samples were salt rock (NaCl) and glauberite ($Na_2SO_4{\cdot}CaSO_4$), with contents of 89.6% and 3.6%, respectively. The sample weighed 3,112.47 g with a density of 2.2 g/cm^3. The salt rock sample is a standard cylindrical sample with a 200 mm height and 100 mm diameter. To minimize damage to the rock framework during the drilling process, a KDXQ-II instrument was used for wire cutting. Simultaneously, meticulous grinding was performed on both ends of the sample to minimize the impact of unevenness, controlled within ±0.03 mm. Upon completion of

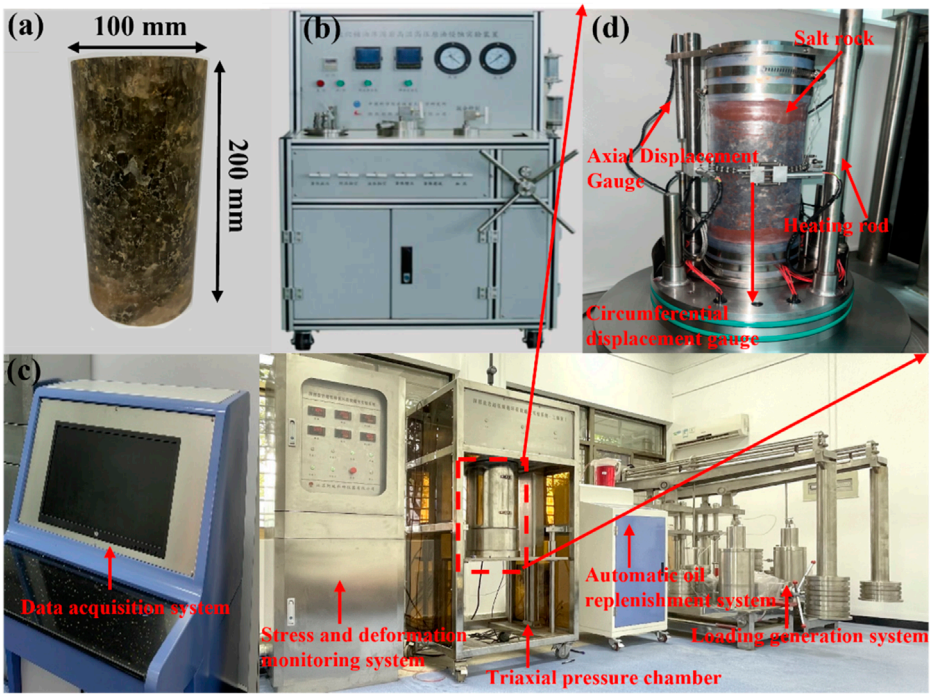

FIGURE 2
(A) salt rock sample; **(B)** test equipment for high-temperature and high-pressure medium soaking of surrounding rock in salt cavern storage; **(C)** deep salt rock ultra-low-frequency cyclic loading creep experimental system; **(D)** installed sample.

the sample processing, wrap it in plastic film to protect against moisture absorption and deliquescence during storage. The salt rock sample is depicted in Figure 2A. The samples for this experiment are taken from the project site. Although the two samples are taken from the same core, there will be a certain degree of difference between the two samples due to the difference in cutting, sample inhomogeneity and transportation environment, which inevitably affects the experimental results to a certain extent. However, the samples at the project site are more meaningful for guiding the actual project. Therefore, this difference is also acceptable.

2.2 Experimental method

The electrolyte soaking treatment of salt rock sample was conducted using a self-developed equipment for high-temperature and high-pressure medium soaking of surrounding rock in salt cavern storage, as illustrated in Figure 2B. This equipment could soak sample with a diameter not exceeding 120 mm and a height not exceeding 250 mm. The static water pressure can reach up to 50 MPa, and the temperature can reach a maximum of 100°C. According to logging results, the ground temperature at a depth of 1,455 m was 58°C. Based on geostress calculations, the geostress at this depth was approximately 28.6 MPa. The acquisition of geostress is obtained through on-site measurements by the China Petroleum Group North China Logging Company. The method used for measuring geostress is the small-scale hydraulic fracturing method. This is a reliable and effective method for measuring deep crustal stress. To emulate the real operating environment of underground SCFB storage as closely as possible, the static water pressure during the electrolyte soaking treatment was set at 30 MPa, with a temperature of 60°C. The erosion duration was 2 days. The weight of the sample after 2 days of soaking at high temperature and pressure is 3,113.63 g, which is 1.16 g heavier than before soaking. This indicated that the electrolyte had permeated the internal defects of the sample, leading to an increase in its weight.

The cyclic loading test was conducted using a self-developed deep salt rock ultra-low-frequency cyclic loading creep experimental system, as depicted in Figure 2C. This system comprised five main components: the triaxial pressure chamber, stress and deformation monitoring system, loading generation system, data acquisition system, and automatic oil replenishment system. The data acquisition system is based on the data acquisition software jointly developed by our organization and Jiangsu Kedi Scientific Research Instrument Co., Ltd. The software can read the signals of stress sensors and displacement sensors and record them according to the time intervals set by the user. The system can apply a maximum confining pressure of about 50 MPa and a maximum axial pressure of 80 MPa, with temperatures reaching up to 100°C. The axial displacement measurement range can reach 50 mm, and the circumferential measurement range can reach 25 mm. Equipped with an uninterruptible power supply, the system can ensure normal operation for over 72 h under power outage conditions. It could fulfill single-cycle periods ranging from 2 h to 6 months.

After the erosion treatment of the sample is completed, immediately remove it and place two equal diameter pressure heads on the upper and lower ends of the sample. Cover with thermoplastic tubing for sealing. Install the circumferential displacement sensor

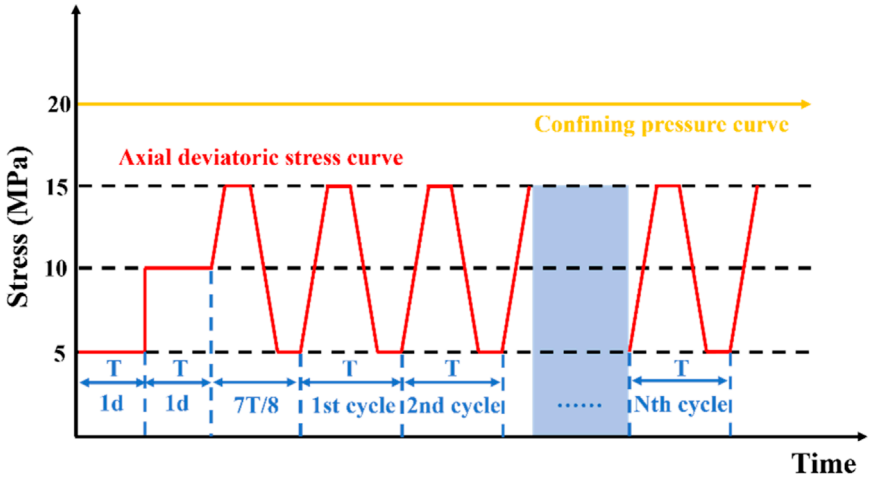

FIGURE 3
Schematic diagram of triaxial long-term cyclic loading waveform.

(Type: FCXA10-005025) and axial displacement sensor (Type: Japanese three quantity digital dial gauge 312–704). Subsequently, the sample is placed in the triaxial chamber of the creep testing system. The installation of samples on the creep test system is illustrated in Figure 2D. Close the three-axis chamber and apply the corresponding temperature. The salt rock sample was equivalent to experiencing unloading at the end of sampling compared to the *in-situ* environment. Thus, to restore the samples to the state of the original formation, a 2-day recovery phase was conducted before the creep test. During this phase, the sample was subjected to a pressure of 30 MPa, provided by static water pressure, while maintaining a temperature of 60°C. Following the conclusion of the recovery phase, as shown in Figure 3, axial deviator stress was initially increased to 5 MPa and held for 1 day, then further increased to 10 MPa and held for another day. This procedure aimed to observe the effect of electrolyte-bearing state on the creep behavior of salt rock sample during the two constant load phases. Upon completion of these two constant load phases, the cyclic loading tests were started.

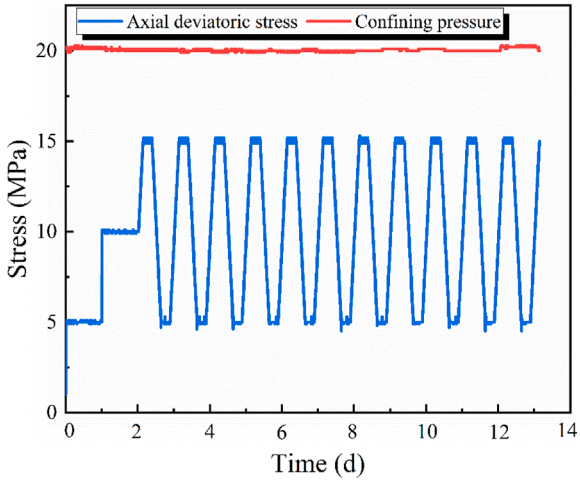

FIGURE 4
Axial deviatoric stress and confining pressure curves with time.

3 Analysis of the test results

3.1 Stress–strain curves

Figure 4 shows the axial deviatoric stress and confining pressure curves with time. The tested confining pressure data showed stabilization at 20 MPa, while the tested axial deviatoric stress data showed smooth and gradual increases and decreases during the slow-rise and slow-fall stages. Minor fluctuations were observed during the constant high and low stress stages, but these fluctuations did not impact the test results. Prior to the commencement of cyclic loading, two constant loading stages (5 and 10 MPa) were applied to sample, each lasting for 1 day. The 5 MPa here refers to the axial deviatoric stress, which is an axial pressure of 25 MPa. Similarly, 10 MPa of axial deviatoric stress is also an axial pressure of 35 MPa. The purpose of these two constant loading stages was to observe the deformation behavior in the electrolyte-bearing and the electrolyte-free states under the same stress environment.

Figure 5 illustrates the axial stress-strain curves for the samples with and without electrolyte under two constant load stages and cyclic load stages. The axial stress-strain curves of samples in two different states. After two constant load stages, axial stress-strain curves of samples with and without electrolyte still exhibit two distinct phases, namely, "sparse-dense". The appearance of this event is analogous to creep experiments performed on uniaxial testing machines (Li Z. et al., 2023). The results obtained in this study also show that the stress-strain curve of the sample under creep test undergoes a "sparse-dense" phase in the early part of the stress-strain curve. The limitations of the samples are explained in section 2.1, so it is assumed that this phenomenon is not due to the differences

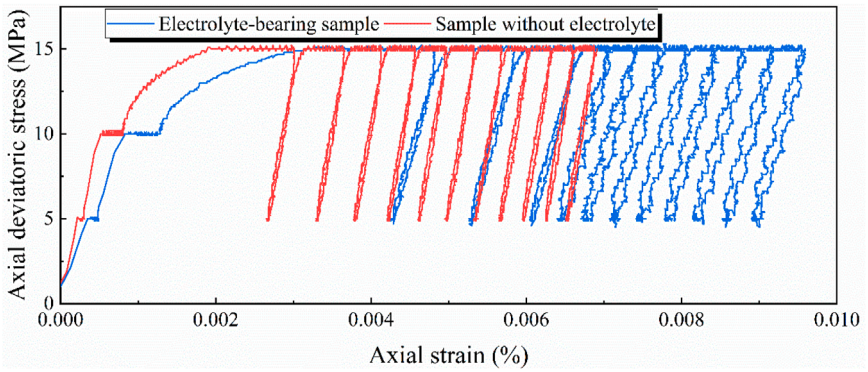

FIGURE 5
The axial stress-strain curves for the samples with and without electrolyte under two constant load stages and cyclic load stages.

in the samples, but rather that applying the constant loading before the cyclic loading does not alter the fundamental characteristics of the fatigue curve. The stress-strain curves of both the samples with and without electrolyte appear to be sparse in the early part of the experiment period, which is due to the large amount of strain accumulation during the constant loading phase. During the creep experimental stage, strain increment gradually stabilizes, resulting in the stress-strain curve approaching denser values. Additionally, the stress-strain curve of the electrolyte-bearing sample undergoes a "dense" stage approximately 4 cycles earlier than that of the sample without electrolyte.

Figure 6A shows the axial strain as a function of time for electrolyte-bearing sample and sample without electrolyte. During the initial application of two constant loading stages, the strain of electrolyte-bearing sample exceeds that of sample without electrolyte. This trend persists during the cyclic loading phase. This suggests that the state of electrolyte-bearing promotes further development of defects (pores or cracks) within the salt rock sample, resulting in poorer densification and enhanced deformability. By selecting 1 day as an observation period, the strain differences between the two types of samples were compared, as illustrated in Figure 6B and Table 1. With increasing time, the deformation of electrolyte-bearing sample significantly surpasses that of sample without electrolyte, exhibiting a trend of rapid increase followed by gradual stabilization. In order to further analyze the strain fluctuations of the electrolyte-bearing and without electrolyte samples on different days, the variance of each was calculated. The variance of the electrolyte-bearing sample is 6.41×10^{-6} and the variance of the without electrolyte sample is 3.56×10^{-6}. This indicates that the strain data of the electrolyte-bearing sample is more volatile, which may be attributed to the fact that the sample contains electrolyte, which leads to a change in the internal pore structure, causing its strain to be more volatile.

3.2 Stress–strain curve in a single cycle

Since Figure 5 depicts complete axial stress-strain curve of creep experiment, it appears to be somewhat dense. In order to more clearly analyze the difference between the creep deformation of the samples in two different states, the stress-strain curves within a single cycle are plotted. Taking the electrolyte-bearing sample as an example, the axial stress-strain curves are plotted (Figure 7).

From Figure 7, the stress-strain curves of electrolyte-bearing sample exhibit different phases, and in order to subdivide them even further, the complete curves are divided into a total of six phases. This characterization of different phase is generally similar to that of the sample without electrolyte. In particular, at the initial loading stage of the creep experiment, the axial stress-strain curve in a single cycle can be further subdivided into two stages. One is the elastic deformation, whose slope is approximately linear, and the resulting deformation belongs to the elastic deformation, which is the stage I labeled in the Figure 7. The other is the plastic deformation, and the resulting deformation belongs to the irreversible deformation, which is the stage II labeled in the Figure 7. In the stage I, creep deformation increases in a nearly linear manner with increasing axial stress. In stage II, creep deformation of sample increases faster, and axial stress-strain curve gradually tends to be horizontal. It is noteworthy that as the cycle number increases, the strain in stage II gradually decreases and disappears in the 4th cycle, whereas for sample without electrolyte, stage II disappears in the 17th cycle. Stage III represents the constant high stress phase, where the stress remains constant at the highest cyclic load, while the strain continues to increase. In stage IV, the changes in axial stress do not have an effect on the axial strain of electrolyte-bearing sample. The reason for this phenomenon is that the elastic recovery deformation due to stress reduction offsets the creep deformation at that stress, so the overall axial strain remains constant. In stage V, the decreasing axial stress triggers an elastic recovery of the axial strain. Stage VI represents the constant low stress phase, where the stress remains constant at the lowest cyclic stress, and the strain remains essentially unchanged.

Figure 8 illustrates variation of axial strain of electrolyte-bearing sample in different stage with number of cycles. As shown in Figure 8A, axial strain remains relatively constant throughout stages I, IV, V, and VI no matter the cycle number. Moreover, axial strain is nearly 0 during stages IV and VI, indicating minimal or no change in axial strain during the two stages. Observation shows that axial strain developed in stage I and

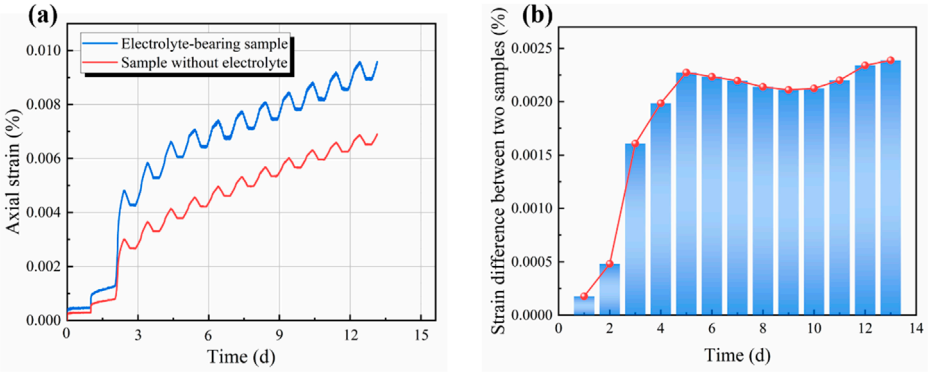

FIGURE 6
(A) Axial strain of samples in two different states with time, **(B)** the strain differences between the samples in two different states.

TABLE 1 Strain difference between the samples in two different states.

Time (d)	Strain of electrolyte-bearing sample (%)	Strain of sample without electrolyte (%)	Strain difference (%)
1	4.736×10^{-4}	2.960×10^{-4}	1.776×10^{-4}
2	1.287×10^{-3}	8.041×10^{-4}	4.829×10^{-4}
3	4.288×10^{-3}	2.680×10^{-3}	1.608×10^{-3}
4	5.296×10^{-3}	3.310×10^{-3}	1.986×10^{-3}
5	6.064×10^{-3}	3.790×10^{-3}	2.274×10^{-3}
6	6.444×10^{-3}	4.210×10^{-3}	2.234×10^{-3}
7	6.807×10^{-3}	4.610×10^{-3}	2.197×10^{-3}
8	7.119×10^{-3}	4.980×10^{-3}	2.139×10^{-3}
9	7.461×10^{-3}	5.350×10^{-3}	2.111×10^{-3}
10	7.794×10^{-3}	5.670×10^{-3}	2.124×10^{-3}
11	8.161×10^{-3}	5.960×10^{-3}	2.201×10^{-3}
12	8.590×10^{-3}	6.250×10^{-3}	2.340×10^{-3}
13	8.899×10^{-3}	6.510×10^{-3}	2.389×10^{-3}

that developed in stage V are comparatively close to each other, which indicates that the creep deformation in these two stages belongs to elastic deformation. This also means that the elastic deformation generated by loading stage is basically recovered in unloading stage.

From Figure 8B, it can be observed that if the stages II and III are viewed as a whole, the axial strains developed by them exhibit a two-phase pattern characterized by a "gradual decrease-basically stabilization" trend with cycles. Since the axial strain developed during stage I by the electrolyte-bearing sample is essentially elastic strain, this part of strains are recovered during stage V. Consequently, the axial strain developed in this whole should be attributed to plastic deformation. Electrolyte-bearing sample becomes progressively denser as further progress in the creep experiments increases, resulting in a gradual reduction in the plastic deformation generated during each cycle. By the 4th cycle, stage II disappears, and the axial strain during stage III approaches 0.0003. This value is approximately twice the axial strain convergence value observed during stage III for the sample without electrolyte.

3.3 Creep strain and creep rate

Figure 9A depicts the creep strain and creep rate of electrolyte-bearing sample as a function of time. The creep rate of electrolyte-bearing sample exhibits periodic fluctuations with variations of axial

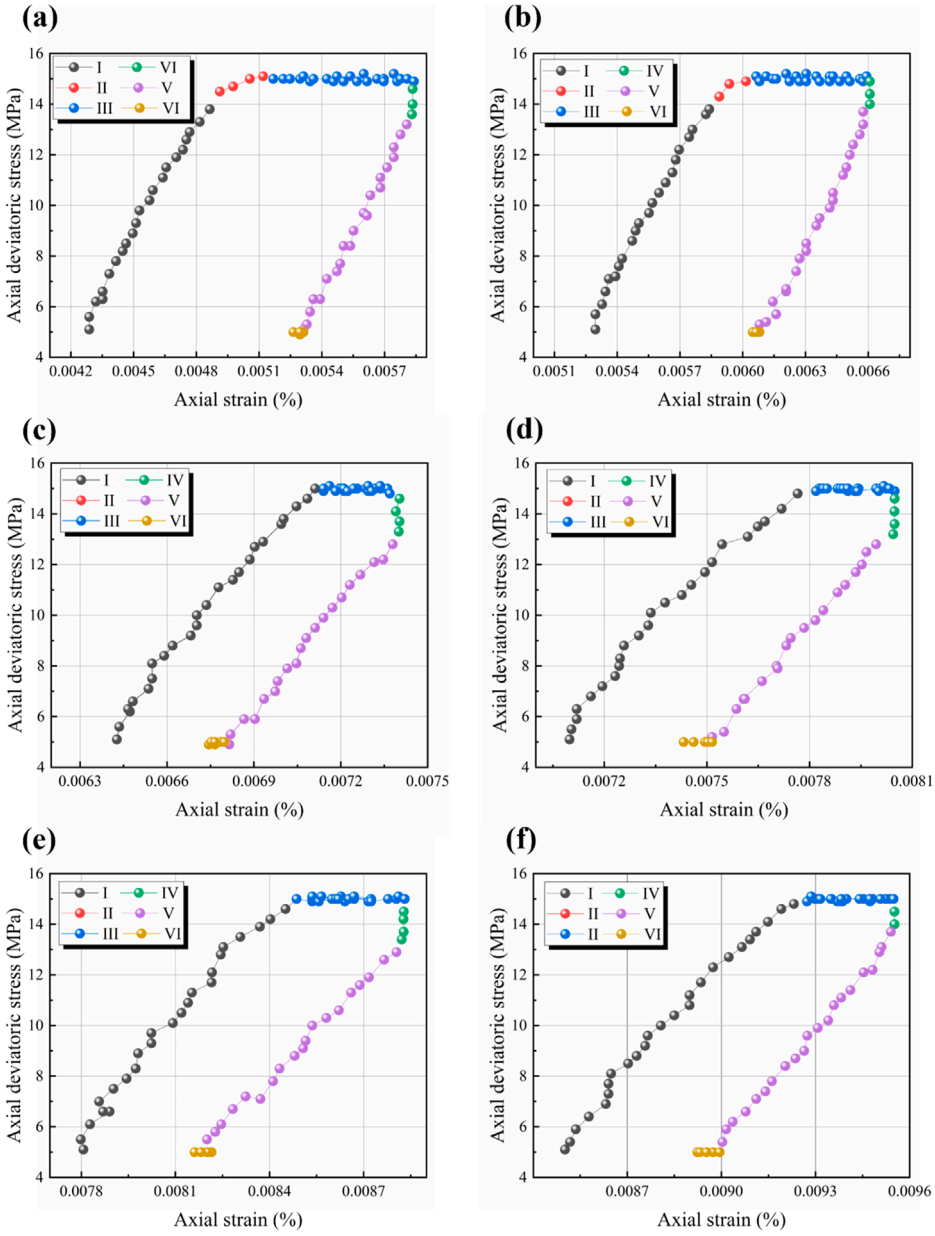

FIGURE 7
Axial stress-strain curves of electrolyte-bearing sample. **(A)** 1st cycle; **(B)** 2nd cycle; **(C)** 4th cycle; **(D)** 6th cycle; **(E)** 8th cycle; **(F)** 10th cycle.

stress owing to the cyclic loading. As the creep experiments are carried out further, it is observed that at the stage of unloading to the minimum cyclic stress level, the creep rate reaches a minimum and remains relatively constant (indicated by the red dots in Figure 9A). When the cyclic stress level reaches its maximum during the creep experiment, the creep rate at this point follows a "gradual decrease—basically stabilization" trend (indicated by yellow dots in Figure 9A). Based on the observed variations in the maximum creep rate of electrolyte-bearing sample from loading to the undamaged, the creep process can be divided into two stages. One is decay creep stage, in which maximum creep rate of the sample gradually decreases with time. The other is steady creep stage, in which maximum creep rate of the sample remains relatively constant.

The creep rate curve in Figure 9A is densely plotted, making it difficult to intuitively discern the variation pattern of creep rate of electrolyte-bearing sample within a single cycle. Therefore, plots depicting the variations of creep rate, axial strain, and axial deviatoric stress over time for the 3rd and 4th cycles are illustrated in Figure 9B. Within a complete cycle, stress variation comprises four stages: (i) load increasing stage, (ii) constant high stress stage, (iii) load decreasing stage, and (iv) constant low stress stage. Correspondingly, creep rate also exhibits four stages within a cycle: (i) during the load increasing stage, creep

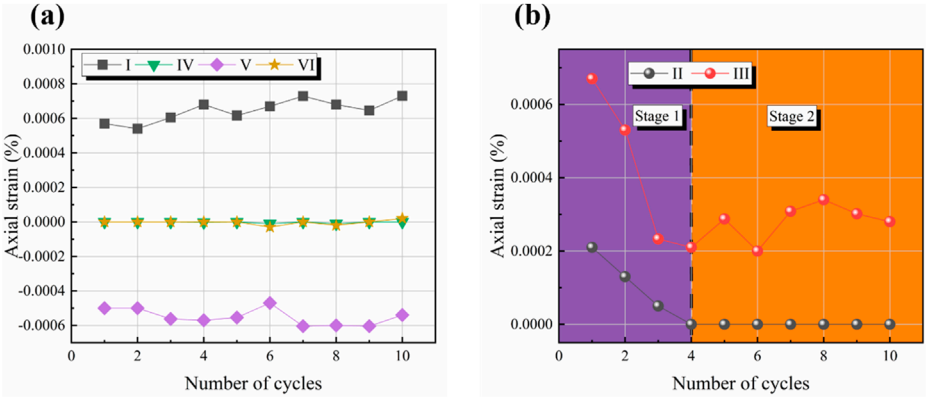

FIGURE 8
Variation of axial strain of electrolyte-bearing sample in different stage. **(A)** Stage I, stage IV, stage V and stage VI, **(B)** stage II and stage III.

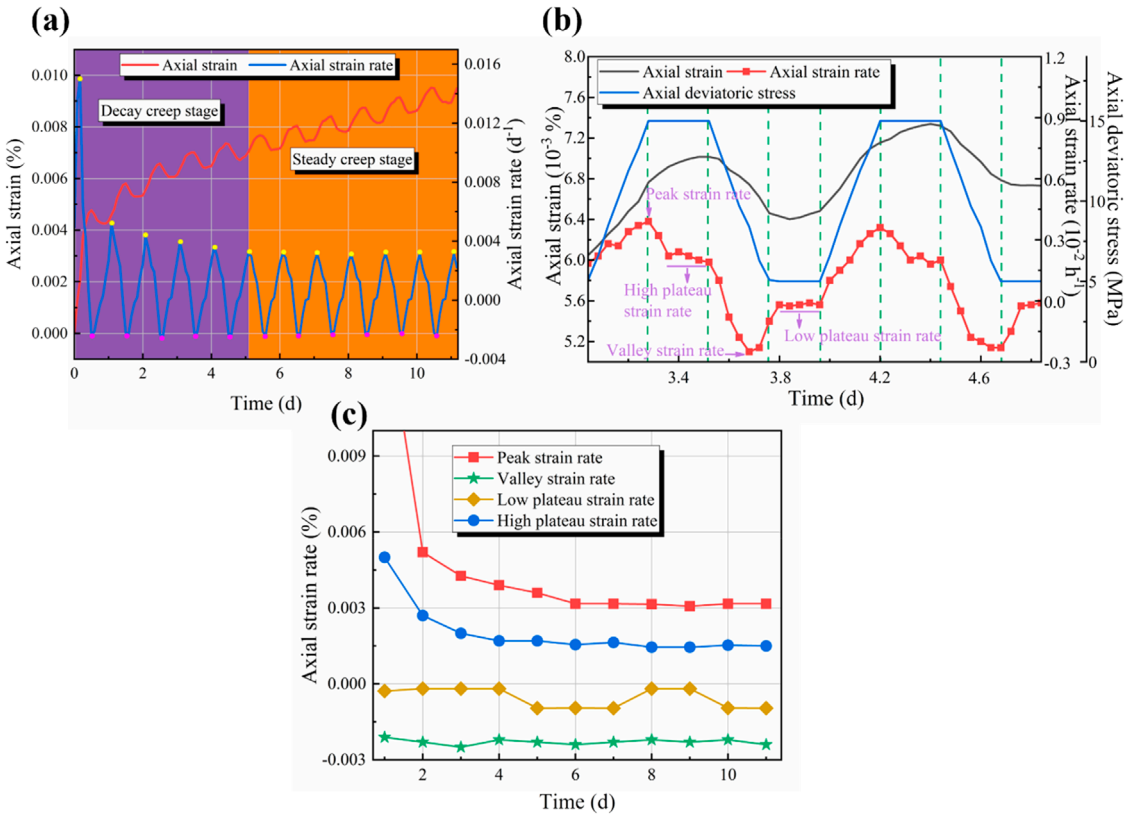

FIGURE 9
Creep rate of the electrolyte-bearing sample. **(A)** variations of creep strain and creep rate over time; **(B)** variations of creep rate, axial strain, and axial deviatoric stress over time for the 3rd and 4th cycles; **(C)** variations curves of peak, valley, high plateau, and low plateau strain rate over time.

rate gradually increases, and in the load to reach the maximum cyclic load creep rate reaches its maximum. At the meantime, the creep rate of electrolyte-bearing sample also reaches the peak of fluctuation curve, which can be referred to as the peak strain rate of the cycle; (ii) during the constant high stress stage, the creep rate curve rapidly decreases from the peak strain rate to a "plateau", where the strain rate stabilizes, termed as the high plateau strain rate; (iii) during load decreasing stage, creep rate gradually decreases, and the speed of the decreasing gradually decreases over time until the axial stress approaches the minimum cyclic load, at which point the creep rate minimizes, also representing minimum of creep rate fluctuation curve for that cycle, termed as the valley strain rate; (iv) during the constant low stress stage, the creep rate curve rapidly rises from the valley strain rate to a "plateau", where the strain rate stabilizes, termed as the low plateau strain rate.

Figure 9C illustrates the variations curves of peak, valley, high plateau, and low plateau strain rate over time for electrolyte-bearing sample. As depicted, both peak and high plateau exhibit a trend of "gradual decrease—basically stabilization" over cycles, while valley strain rate fluctuates slightly around a certain constant negative value. The average valley strain rate for electrolyte-bearing sample is −0.0023/d, which is lower by −0.0005/d compared to the average valley strain rate for sample without electrolyte. The low plateau strain rate for electrolyte-bearing sample is essentially equal to 0, similar to the case for sample without electrolyte.

3.4 Elastic modulus

The elastic modulus plays an essential role in assessing elastic deformation of electrolyte-bearing sample. The elastic modulus E of a sample within a given single cycle is taken from the slope of the linear segment during initial cyclic pressure increase phase, which is also the slope of linear segment in the stage I. Figure 10 displays the evolution of elastic modulus of electrolyte-bearing sample over cycles. As shown in Figure 10, the elastic modulus of electrolyte-bearing sample exhibits a gradual increase in the stage 1 as the creep experiment continues. This is followed by a stabilizing trend in the stage 2. The elastic modulus of the electrolyte-bearing sample shows a gradual increase trend throughout the first four cycles of overall creep experiment. Starting from the fourth cycle, the elastic modulus of electrolyte-bearing sample tends to reach a stable stage (stage 2), where it fluctuates but maintains an overall stability without a noticeable increasing or decreasing trend. Taking an average of all the elastic modulus values for the electrolyte-bearing sample in stage 2, the value is calculated to be 12.61 GPa, which is about half of the value for stage 2 of sample without electrolyte. The above analysis shows that the creep rate of electrolyte-bearing sample is larger than that of sample without electrolyte (Dong, 2023), and the time to enter the stable creep rate is shorter. This indicates that the creep characteristics of the electrolyte-bearing sample should be fully considered when designing the SCFB system. In particular, when designing the parameters of the operating pressure range inside the salt cavern, it is recommended to increase the maximum operating pressure or shorten the low stress time inside the salt cavern. This will be of great significance to ensure the stability of the SCFB storage.

Salt rock, as a rock precipitated by evaporating seawater or lake action, contains a certain amount of internal defects such as pores or cracks. After soaking in electrolyte, these internal pores or cracks undergo further development, which is an essential factor contributing to the variations of the elastic modulus of electrolyte-bearing sample in creep experiments. Typically, the elastic modulus of rocks decreases with an increase in microscopic defects, and *vice versa*. In the initial stages of cyclic loading for electrolyte-bearing sample, the microscopic defects inside the sample gradually tend to close, causing an increase in densification and an enhancement of the resistance to deformation. This is fed back into the increasing trend of the elastic modulus (stage 1). When creep experiment reaches a certain level, the sample has been compressed to near its limit, which also means that the density of sample is approaching its maximum value. At this point, elastic modulus of sample no longer changes significantly as number of cycle increases, indicating that elastic modulus of sample tends to stabilize (stage 2).

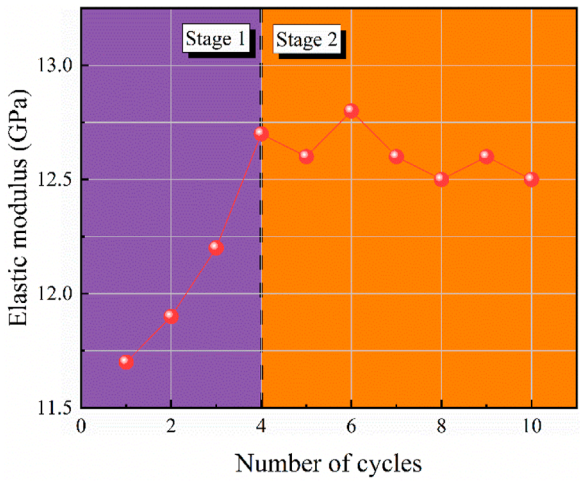

FIGURE 10
The elastic modulus of electrolyte-bearing sample over cycles.

3.5 Irreversible deformation

The axial strain generated during each cycle is made up of elastic deformation (reversible) and plastic deformation (irreversible). From the previous analysis, it has been known that axial deformation developed in stage I is elastic in nature, this part of deformation essentially recovers in stage V of unloading. However, axial deformation developed in stages II and III are plastic deformation, which are irreversible, and therefore this part of deformation is not recovered. The plastic deformation has an essential impact on fatigue behavior (Zhao et al., 2022). The irreversible deformation within a single cycle is calculated by subtracting the strain at the beginning and end of the cycle. Figure 11 shows the variation of irreversible deformation of electrolyte-bearing sample over cycles. When the salt rock sample is not loaded to destruction, the changes in cumulative irreversible deformation can be categorized into two stages over cycles. One is attenuation phase, in which the irreversible deformation gradually decreases over a cycle. The other is stable stage, in which the irreversible deformation remains essentially constant over a cycle.

The irreversible deformation includes plastic deformation during loading stage (stage II) and creep deformation during high constant stress stage (stage III). As shown in Figure 8B, both stages exhibit a characteristic of gradually decreasing with increasing number of cycles until reaching a stable state, indicating that the irreversible deformation also exhibits a two-phase characteristic of "gradual decrease-basically stabilization" as number of cycles increase. Compared to the deformation in stage III, the deformation in stage II constitutes a lesser percentage of the irreversible deformation, and the deformation in stage II disappears in the 4th cycle, indicating that irreversible deformation in cyclic loading is mainly generated during the high constant stress stage (stage III).

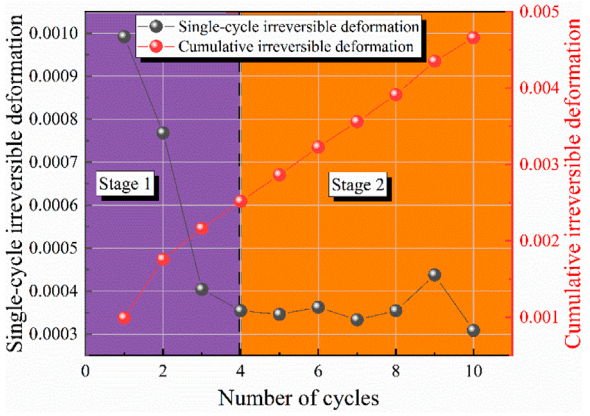

FIGURE 11
The variation of irreversible deformation of electrolyte-bearing sample over cycles.

4 Conclusion

To study the creep characteristics of electrolyte-bearing salt rock in a SCFB system under long-term cyclic loading, creep tests with a cycle period of 1 day were conducted. The effect of the electrolyte state on the creep characteristics of salt rock sample is comparatively analyzed. Based on the scope of this study, the following conclusions can be drawn:

(1) The axial stress-strain curve of the electrolyte-bearing sample undergoes only two phases of "sparse-dense" when not been loaded to the failure point, which is similar to the results of creep experiments of sample without electrolyte. The electrolyte-bearing sample undergoes a "dense" stage approximately 4 cycles earlier than sample without electrolyte.

(2) In the two constant stress stages (5 and 10 MPa) and cyclic loading stage, the strain of electrolyte-bearing sample is greater than that of sample without electrolyte. The trend presented is to increase rapidly in the 5th cycles, and then gradually stabilize.

(3) The axial stress-strain curve of electrolyte-bearing sample over a cycle could be divided into six stages, which is similar to that of sample without electrolyte. The axial strain in stages I, IV, V and VI is essentially cycle independent. The axial strain in stages IV and VI is basically 0. The elastic deformation developed in stage I is basically recovered in stage V. The strain in stage II gradually decreases and disappears in the 4th cycle.

(4) Under cyclic loading, the creep rate of electrolyte-bearing sample exhibits periodic fluctuations with variations of axial stress. When the cyclic stress level reaches its maximum during the creep experiment, the creep rate at this point follows a "gradual decrease—basically stabilization" trend. When not loaded to the point of failure, the creep process of the electrolyte-bearing sample includes only two stages: the decay creep and steady creep stages.

(5) The elastic modulus of electrolyte-bearing sample gradually increases over cycles. From the 4th cycle, the elastic modulus tends to a stable phase. The overall trend is "gradually increasing - basically stabilization". The average value of elastic modulus of electrolyte-bearing sample during the stable phase is 12.61 GPa, which is about half that of the sample without electrolyte.

(6) The irreversible deformation exhibits a two-phase characteristic of "gradual decrease-basically stabilization" with increasing number of cycles, mainly generated in stage III. When the electrolyte-bearing salt rock is not damaged, the cumulative irreversible deformation over cycles can be divided into two phases: attenuation and stable phases.

The results of this study deepen our understanding of the influence of electrolyte-bearing states on the creep characteristics of salt rock, facilitating a systematic comprehension of the creep behavior of rock salt in salt caverns as a storage site for electrolyte. This research provides crucial experimental and theoretical foundations for the parameter design and stability analysis of SCFB system. As the SCFB reservoir may have a longer cycling cycle and be subjected to more complex loads during operation, in order to further investigate the creep behavior of electrolyte-bearing salt rock, future research may consider carrying out ultra-low frequency cyclic load creep experiments with longer cycling cycles and more complex waveforms, so as to better serve the engineering site.

Data availability statement

The original contributions presented in the study are included in the article/supplementary material, further inquiries can be directed to the corresponding author.

Author contributions

SH: Conceptualization, Data curation, Investigation, Methodology, Writing–original draft. JL: Investigation, Visualization, Writing–review and editing. JW: Investigation, Visualization, Writing–review and editing. XiF: Investigation, Visualization, Writing–review and editing. YF: Investigation, Visualization, Writing–review and editing. YL: Conceptualization, Project administration, Resources, Supervision, Writing–review and editing. XS: Conceptualization, Methodology, Project administration, Resources, Supervision, Writing–review and editing. ZD: Data curation, Investigation, Visualization, Writing–review and editing. KZ: Visualization, Writing–review and editing. PL: Visualization, Writing–review and editing. MX: Visualization, Writing–review and editing. XC: Visualization, Writing–review and editing.

Funding

The author(s) declare that financial support was received for the research, authorship, and/or publication of this article. This work was financially supported by the Excellent Young Scientists Fund Program of National Natural Science Foundation of China (No. 52122403), Youth Innovation Promotion Association of Chinese

Academy of Sciences (No. Y2023089), National Natural Science Foundation of China (No. 52374069, No. 52304069, No. 52304070 and No. 52208342), and supported by Jiangxi Provincial Natural Science Foundation (20242ACB214008, 20232BAB204072).

Conflict of interest

Authors JL, JW, and YF were employed by PipeChina Energy Storage Technology Co., Ltd. Author XF was employed by Jiangsu Suyan Jingshen Co., Ltd.

The remaining authors declare that the research was conducted in the absence of any commercial or financial relationships that could be construed as a potential conflict of interest.

Generative AI statement

The author(s) declare that no Generative AI was used in the creation of this manuscript.

Publisher's note

All claims expressed in this article are solely those of the authors and do not necessarily represent those of their affiliated organizations, or those of the publisher, the editors and the reviewers. Any product that may be evaluated in this article, or claim that may be made by its manufacturer, is not guaranteed or endorsed by the publisher.

References

Ambrose, B., Naresh, R., Deshmukh, S., Kathiresan, M., and Ragupathy, P. J. E. (2023). Exploring contemporary advancements and outlook in viologen-based aqueous organic redox flow batteries: a mini review. *Energy and Fuels* 37, 18226–18242. doi:10.1021/acs.energyfuels.3c02299

Bao, C., Tong, M., Li, X., and Xiang, Z. (2024). d-Orbital steered FeN4 moiety through N, S dual-site adjustation for zinc-air flow battery. *J. Energy Chem.* 92, 8–15. doi:10.1016/j.jechem.2024.01.035

Beh, E. S., De Porcellinis, D., Gracia, R. L., Xia, K. T., Gordon, R. G., and Aziz, M. J. (2017). A neutral pH aqueous organic–organometallic redox flow battery with extremely high capacity retention. *ACS Energy Lett.* 2, 639–644. doi:10.1021/acsenergylett.7b00019

Bérest, P., Gharbi, H., Brouard, B., Brückner, D., DeVries, K., Hévin, G., et al. (2019). Very slow creep tests on salt samples. *Rock Mech. Rock Eng.* 52, 2917–2934. doi:10.1007/s00603-019-01778-9

Cao, J., Tian, J., Xu, J., and Wang, Y. J. E. (2020). Organic flow batteries: recent progress and perspectives. *Energy and Fuels* 34, 13384–13411. doi:10.1021/acs.energyfuels.0c02855

Cao, Z., Sun, Q., Li, Z., and Du, F. (2024a). Abnormal ore pressure mechanism of working face under the influence of overlying concentrated coal pillar. *Sci. Rep.* 14, 626. doi:10.1038/s41598-024-51148-x

Cao, Z., Wang, P., Li, Z., and Du, F. (2024b). Migration mechanism of grouting slurry and permeability reduction in mining fractured rock mass. *Sci. Rep.* 14, 3446. doi:10.1038/s41598-024-51557-y

Cao, Z., Yang, X., Li, Z., and Du, F. (2024c). Evolution mechanism of water-conducting fractures in overburden under the influence of water-rich fault in underground coal mining. *Sci. Rep.* 14, 5081. doi:10.1038/s41598-024-54803-5

Cao, Z., Yang, X., Li, Z., Huang, C., Du, F., Wang, W., et al. (2024d). Fracture propagation and pore pressure evolution characteristics induced by hydraulic and pneumatic fracturing of coal. *Sci. Rep.* 14, 9992. doi:10.1038/s41598-024-60873-2

Cao, Z., Yang, X., Zhang, P., Li, Z., Du, F., Wang, W., et al. (2024e). Experimental study on the fracture surface morphological characteristics and permeability characteristics of sandstones with different particle sizes. *Energy Sci. and Eng.* 12, 2798–2809. doi:10.1002/ese3.1768

Chen, J., Ren, S., Yang, C., Jiang, D., and Li, L. (2013). Self-healing characteristics of damaged rock salt under different healing conditions. *Materials* 6, 3438–3450. doi:10.3390/ma6083438

Chen, Q., Lv, Y., Yuan, Z., Li, X., Yu, G., Yang, Z., et al. (2021). Organic electrolytes for pH neutral aqueous organic redox flow batteries. *Adv. Funct. Mater.* 32. doi:10.1002/adfm.202108777

DeBruler, C., Hu, B., Moss, J., Liu, X., Luo, J., Sun, Y., et al. (2017). Designer two-electron storage viologen anolyte materials for neutral aqueous organic redox flow batteries. *Chem* 3, 961–978. doi:10.1016/j.chempr.2017.11.001

Dong, Z. (2023). Study on creep test and constitutive model of salt rock under complex loading. Doctoral thesis.

Dong, Z., Li, Y., Li, H., Wang, Z., Shi, X., Chen, X., et al. (2023). Experimental study on the influence of temperature on rock salt creep. *Rock Mech. Rock Eng.* 56, 3499–3518. doi:10.1007/s00603-023-03219-0

Dunn, B., Kamath, H., and Tarascon, J. M. (2011). Electrical energy storage for the grid: a battery of choices. *Science* 334, 928–935. doi:10.1126/science.1212741

Fan, J., Chen, J., Jiang, D., Chemenda, A., Chen, J., and Ambre, J. (2017). Discontinuous cyclic loading tests of salt with acoustic emission monitoring. *Int. J. Fatigue* 94, 140–144. doi:10.1016/j.ijfatigue.2016.09.016

Fan, J., Chen, J., Jiang, D., Ren, S., and Wu, J. (2016). Fatigue properties of rock salt subjected to interval cyclic pressure. *Int. J. Fatigue* 90, 109–115. doi:10.1016/j.ijfatigue.2016.04.021

Fuenkajorn, K., and Phueakphum, S. D. J. S. J. o. (2009). Effects of cyclic loading on mechanical properties of maha sarakham salt. *Eng. Geol.* 112, 43–52. doi:10.1016/j.enggeo.2010.01.002

Gentil, S., Reynard, D., and Girault, H. H. (2020). Aqueous organic and redox-mediated redox flow batteries: a review. *Curr. Opin. Electrochem.* 21, 7–13. doi:10.1016/j.coelec.2019.12.006

Guessous, Z., Gill, D. E., and Ladanyi, B. (1987). Effect of simulated sampling disturbance on creep behaviour of rock salt. *Rock Mech. Rock Eng.* 20, 261–275. doi:10.1007/bf01024645

Hongwei, Z., Di, L., Gang, L., Dongjie, X., and Yang, Z. (2018). The creep-damage model of salt rock based on fractional derivative. *Energies* 11, 2349. doi:10.3390/en11092349

Huang, L., Fang, Y., Hou, Z., Xie, Y., Wu, L., Luo, J., et al. (2023). A preliminary site selection system for underground hydrogen storage in salt caverns and its application in Pingdingshan, China. *Deep Undergr. Sci. Eng.* 3, 117–128. doi:10.1002/dug2.12069

Kolano, M., Cała, M., and Stopkowicz, A. (2024). Mechanical properties of rock salt from the kłodawa salt dome—a statistical analysis of geomechanical data. *Materials* 17, 3564. doi:10.3390/ma17143564

Kwabi, D. G., Ji, Y., and Aziz, M. J. (2020). Electrolyte lifetime in aqueous organic redox flow batteries: a critical review. *Chem. Rev.* 120, 6467–6489. doi:10.1021/acs.chemrev.9b00599

Li, H., He, Y., Xu, Q., Deng, J., Li, W., and Wei, Y. (2022a). Detection and segmentation of loess landslides via satellite images: a two-phase framework. *Landslides* 19, 673–686. doi:10.1007/s10346-021-01789-0

Li, H., He, Y., Xu, Q., Deng, J., Li, W., Wei, Y., et al. (2022b). Sematic segmentation of loess landslides with STAPLE mask and fully connected conditional random field. *Landslides* 20, 367–380. doi:10.1007/s10346-022-01983-8

Li, H., Ma, H., Yang, C., Zhao, K., Hu, Z., and Daemen, J. J. K. (2023a). Acoustic emission characteristics of rock salt under multi-stage cyclic loading. *Int. J. fatigue* 176, 107911. doi:10.1016/j.ijfatigue.2023.107911

Li, H., Xu, Q., He, Y., and Deng, J. (2018). Prediction of landslide displacement with an ensemble-based extreme learning machine and copula models. *Landslides* 15, 2047–2059. doi:10.1007/s10346-018-1020-2

Li, H., Xu, Q., He, Y., Fan, X., and Li, S. (2019a). Modeling and predicting reservoir landslide displacement with deep belief network and EWMA control charts: a case study in Three Gorges Reservoir. *Landslides* 17, 693–707. doi:10.1007/s10346-019-01312-6

Li, J., Yang, C., Shi, X., Xu, W., Li, Y., and Daemen, J. J. K. (2020). Construction modeling and shape prediction of horizontal salt caverns for gas/oil storage in bedded salt. *J. Petroleum Sci. Eng.* 190, 107058. doi:10.1016/j.petrol.2020.107058

Li, T., Pei, X., Wang, D., Huang, R., and Tang, H. (2019b). Nonlinear behavior and damage model for fractured rock under cyclic loading based on energy dissipation principle. *Eng. Fract. Mech.* 206, 330–341. doi:10.1016/j.engfracmech.2018.12.010

Li, Z., Kang, Y., Fan, J., Fourmeau, M., Jiang, D., and Nelias, D. (2023b). Creep–fatigue mechanical characteristics of salt rocks under triaxial loading: an experimental study. *Eng. Geol.* 322, 107175. doi:10.1016/j.enggeo.2023.107175

Liu, J., Xie, H., Hou, Z., Yang, C., and Chen, L. (2013). Damage evolution of rock salt under cyclic loading in unixial tests. *Acta Geotech.* 9, 153–160. doi:10.1007/s11440-013-0236-5

Liu, Y., Li, Y., Ma, H., Shi, X., Zheng, Z., Dong, Z., et al. (2022). Detection and evaluation technologies for using existing salt caverns to build energy storage. *Energies* 15, 9144. doi:10.3390/en15239144

Lyu, C., Liu, J., Ren, Y., Liang, C., and Liao, Y. (2021). Study on very long-term creep tests and nonlinear creep-damage constitutive model of salt rock. *Int. J. Rock Mech. Min. Sci.* 146, 104873. doi:10.1016/j.ijrmms.2021.104873

Ma, H., Wei, X., Shi, X., Liang, X., Bai, W., and Ge, L. (2022). Evaluation methods of salt pillar stability of salt cavern energy storage. *Energies* 15, 7570. doi:10.3390/en15207570

Ma, L.-J., Liu, X.-Y., Wang, M.-Y., Xu, H.-F., Hua, R.-P., Fan, P.-X., et al. (2013). Experimental investigation of the mechanical properties of rock salt under triaxial cyclic loading. *Int. J. Rock Mech. Min. Sci.* 62, 34–41. doi:10.1016/j.ijrmms.2013.04.003

McGlade, C., and Ekins, P. (2015). The geographical distribution of fossil fuels unused when limiting global warming to 2°C. *Nature* 517, 187–190. doi:10.1038/nature14016

Mishra, N., and Makov, G. (2022). A novel interstitial site in binary rock-salt compounds. *Materials* 15, 6015. doi:10.3390/ma15176015

Montero, J., da Silva Freitas, W., Mecheri, B., Forchetta, M., Galloni, P., Licoccia, S., et al. (2022). A neutral pH aqueous redox flow battery based on sustainable organic electrolytes. *ChemElectroChem* 10. doi:10.1002/celc.202201002

Peng, H., Fan, J., Zhang, X., Chen, J., Li, Z., Jiang, D., et al. (2020). Computed tomography analysis on cyclic fatigue and damage properties of rock salt under gas pressure. *Int. J. Fatigue* 134, 105523. doi:10.1016/j.ijfatigue.2020.105523

Shi, X., Huang, S., Li, Y., Ma, H., Yang, C., and Li, P. (2023). Salt cavern flow battery system. *U. S. Pat.*, 18–347529.

Shi, X., Liu, W., Chen, J., Jiang, D., Wu, F., Zhang, J., et al. (2018). Softening model for failure analysis of insoluble interlayers during salt cavern leaching for natural gas storage. *Acta Geotech.* 13, 801–816. doi:10.1007/s11440-018-0666-1

Vandeginste, V., Ji, Y., Buysschaert, F., and Anoyatis, G. (2023). Mineralogy, microstructures and geomechanics of rock salt for underground gas storage. *Deep Undergr. Sci. Eng.* 2, 129–147. doi:10.1002/dug2.12039

Voznesenskii, A. S., Krasilov, M. N., Kutkin, Y. O., Tavostin, M. N., and Osipov, Y. V. (2017). Features of interrelations between acoustic quality factor and strength of rock salt during fatigue cyclic loadings. *Int. J. Fatigue* 97, 70–78. doi:10.1016/j.ijfatigue.2016.12.027

Wang, H., Li, D., Xu, J., Wu, Y., Cui, Y., and Chen, L. (2021a). An unsymmetrical two-electron viologens anolyte for salt cavern redox flow battery. *J. Power Sources* 492, 229659. doi:10.1016/j.jpowsour.2021.229659

Wang, J., Xie, H., Leung, C., and Li, X. (2023). A research on excavation compensation theory for large deformation disaster control and a review on the multiphysical–multiscale responses of salt rock for underground gas storage. *Deep Undergr. Sci. Eng.* 2, 103–104. doi:10.1002/dug2.12045

Wang, J., Zhang, Q., Song, Z., and Zhang, Y. (2021b). Experimental study on creep properties of salt rock under long-period cyclic loading. *Int. J. Fatigue* 143, 106009. doi:10.1016/j.ijfatigue.2020.106009

Wang, J. B., Liu, X., Zhang, Q., and Song, Z. P. (2022). Analysis of energy evolution characteristics of salt rock under different loading rates. *Front. Earth Sci.* 10. doi:10.3389/feart.2022.829185

Wang, Z., Chen, F., Dong, Z., Li, H., Shi, X., Xu, Z., et al. (2024). Study on the influence of temperature on the damage evolution of hot dry rock in the development of geothermal resources. *Geoenergy Sci. Eng.* 241, 213171. doi:10.1016/j.geoen.2024.213171

Wei, L., Jie, C., Deyi, J., Xilin, S., Yinping, L., Daemen, J. J. K., et al. (2016). Tightness and suitability evaluation of abandoned salt caverns served as hydrocarbon energies storage under adverse geological conditions (AGC). *Appl. Energy* 178, 703–720. doi:10.1016/j.apenergy.2016.06.086

Wei, X., Shi, X., Li, Y., Li, P., Ban, S., Zhao, K., et al. (2023). A comprehensive feasibility evaluation of salt cavern oil energy storage system in China. *Appl. Energy* 351, 121807. doi:10.1016/j.apenergy.2023.121807

Wei, X., Shi, X., Li, Y., Ma, H., Ban, S., Liu, X., et al. (2024). Analysis of the European energy crisis and its implications for the development of strategic energy storage in China. *J. Energy Storage* 82, 110522. doi:10.1016/j.est.2024.110522

Yang, H., Wang, Y., Dai, Y., Zhang, J., and Chen, G. (2023a). On the acoustic attenuation characteristics of sonar detection in the salt-cavern gas storage environment. *Front. Earth Sci.* 10. doi:10.3389/feart.2022.1029946

Yang, Y., Li, Y., Yuan, K., Lu, Z., and Li, G. (2023b). Experimental study on creep failure characteristics of coal mass under multistage stress and construction of prediction model. *Front. Earth Sci.* 10. doi:10.3389/feart.2022.1031604

Zhang, L., Lu, X., Liu, X., Yang, K., and Zhou, H. J. E. (2016). Surface wettability of basal surfaces of clay minerals: insights from molecular dynamics simulation. *Energy and Fuels* 30, 149–160. doi:10.1021/acs.energyfuels.5b02142

Zhang, N., Liu, W., Zhang, Y., Shan, P., and Shi, X. (2020). Microscopic pore structure of surrounding rock for underground strategic Petroleum reserve (SPR) caverns in bedded rock salt. *ENERGIES* 13, 1565. doi:10.3390/en13071565

Zhao, K., Ma, H., Li, Y., Li, P., Dong, Z., Liu, X., et al. (2022). Deformation and damage evolution of rock salt under multilevel cyclic loading with constant stress intervals. *Eng. Fract. Mech.* 260, 108191. doi:10.1016/j.engfracmech.2021.108191

Zhou, A., Li, D., Shao, X., Du, Y., Zhang, Y., Li, B., et al. (2024). Synchronized dual-modified graphite felt electrodes for all-vanadium redox flow batteries with high power density and ultra-long lifespan. *J. Energy Storage* 81, 110501. doi:10.1016/j.est.2024.110501